PROCEEDINGS OF SCIENCE

Investigation of optimal smearing for mesons

Roberto Di Palma,[a,*] **Giuseppe Gagliardi**[b] **and Francesco Sanfilippo**[c]

[a] *Dipartimento di Fisica, Università Roma Tre and INFN, sezione di Roma Tre, Via della Vasca Navale 84, I-00146 Rome, Italy*

[b,c] *INFN, sezione di Roma Tre, Via della Vasca Navale 84, I-00146 Rome, Italy*

E-mail: roberto.dipalma@uniroma3.it

The Wuppertal smearing is a technique that improves the overlap of an interpolating operator with the ground state of a given channel. We study how to implement optimal smearing parameters to isolate the ground state of several flavours of pseudoscalar and vector mesons at rest and with non-zero momentum, by tuning the smearing radius to minimize a functional built in terms of the overlap with the excited states. The smearing radius shows a monotonic increasing behaviour as a function of the reduced constituent masses of the valence quarks of the mesons. We provide parametric dependence of the optimal smearing parameters in terms of the quark masses, which will be helpful for future studies of meson phenomenology.

The 40th International Symposium on Lattice Field Theory (Lattice 2023)
July 31st - August 4th, 2023
Fermi National Accelerator Laboratory

*Speaker

PoS(LATTICE2023)152

1. Introduction

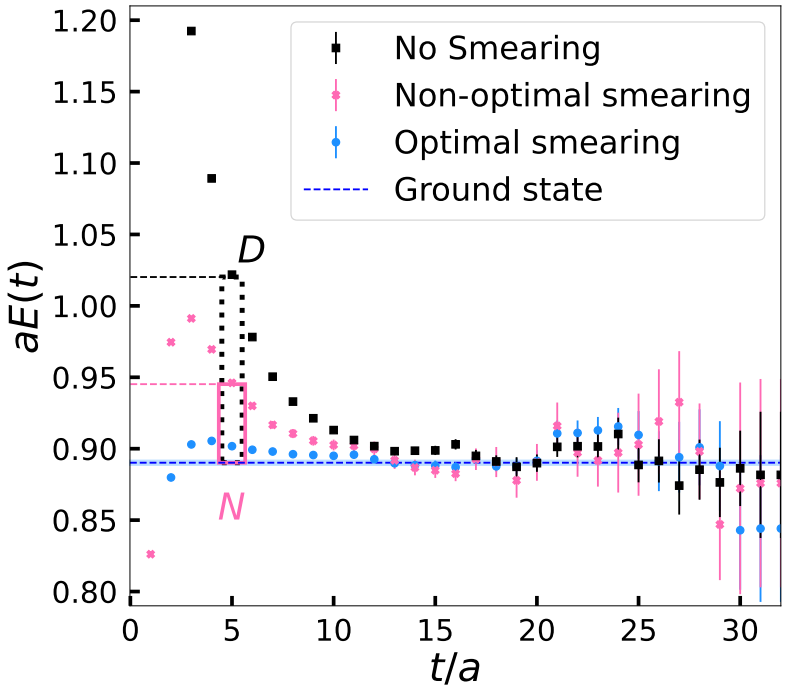

Figure 1: Effective energy for the D meson at rest as a function of the Euclidean time, in lattice units, with no smearing (black), with a non-optimal smearing (pink) and with the optimal smearing (blue). The optimizing strategy for the smearing is described in Sec. 2. The ratio between the effective energy subtracted of the ground state, illustrated by the heights of the N and D rectangles provides an estimate of the efficiency of the smearing at suppressing the excited stated.

Lattice QCD is the only known first-principles method to evaluate hadronic observables. Lattice QCD observables are customarily extracted from the time behaviour of the so-called n point correlation functions at large Euclidean time separation t, where the correlation functions are dominated by the ground state.
Here, we will focus on the problem of isolating the ground states for mesons with three-momentum $\mathbf{p}$, and study two-point functions of the form

$$C(t) = \langle 0| T\{O(t)O^{\dagger}(0)\} |0\rangle = \sum_{m=0}^{\infty} \frac{|\langle 0| O(0) |m\rangle|^2}{2E_m} e^{-E_m t}, \tag{1}$$

where $O(t)$ is an interpolating operator, having the same numbers of the meson of interest, defined in terms of its valence quark fields $q(t,\mathbf{x})$ and $q'(t,\mathbf{x})$ as

$$O(t) = \sum_{\mathbf{x}} e^{i\mathbf{p}\cdot\mathbf{x}} \overline{q}(t,\mathbf{x}) \Gamma q'(t,\mathbf{x}), \tag{2}$$

with $\Gamma = \gamma_5, \gamma^i$, for pseudoscalar and vector mesons, respectively.
The exponential behaviour in the right-most side of Eq. (1) naturally suppresses the contributions

of the excited states at large times, since their energies $E_{m>1}$ are larger than the ground state energy E_0. However, in most cases, the signal-to-noise ratio degrades with increasing time [1, 2], making it very important to anticipate as much as possible the time when the ground state contribution is dominant. As an example of this behavior, we compute the effective energy $E(t)$ of the mesons, defined as the root of the equation

$$\frac{\cosh\left[E(t)(t-T/2)\right]}{\cosh\left[E(t)(t-T/2+a)\right]} = \frac{C(t)}{C(t+a)}, \tag{3}$$

which in the limit of large times t is equal to E_0. In Fig. 1, we report the effective energy for the D meson at rest obtained with and without employing Wuppertal smearing (see discussion below), which becomes very noisy for $t/a > 20$. To isolate the ground state at smaller times, one can modify the interpolating operator to reduce the overlap with the excited states. This is the purpose of the so-called smearing techniques (see for example Refs. [3, 4]).

In this work, we focus on the so-called Wuppertal (Gaussian) smearing, which is an iterative convolution of the so-called smearing operator $G(\mathbf{x},\mathbf{y})$ with a quark field, such that, after n convolution steps, we get

$$q'^{(n)}(t,\mathbf{x}) = \sum_{\mathbf{y}} G^n(\mathbf{x},\mathbf{y}) q'(t,\mathbf{y}), \qquad G(\mathbf{x},\mathbf{y}) = \frac{1}{1+6\kappa}\left[\delta(\mathbf{x},\mathbf{y}) + \kappa \sum_{l=\pm1}^{\pm3} U_l^{\mathrm{APE}}(t,\mathbf{x})\delta(\mathbf{x}+\hat{\mathbf{l}},\mathbf{y})\right]. \tag{4}$$

Here, κ is the intensity of the smearing, while $U_l^{\mathrm{APE}}(t,\mathbf{x})$ are the so-called APE-smeared links [5], that we adopt to keep the parallel transporters aligned as much as possible, which is crucial to obtain Gaussian-distributed quark fields (see the discussion below). The smeared interpolator $O^{(n)}(t)$ is then defined as

$$O^{(n)}(t) = \sum_{\mathbf{x}} e^{i\mathbf{p}\cdot\mathbf{x}} \overline{q^{(0)}}(t,\mathbf{x}) \Gamma q'^{(n)}(t,\mathbf{x}). \tag{5}$$

It is easy to show that using parallel transporters close to the identity and starting from a point-like source located in the origin $q'(t,\mathbf{x}) \propto \delta(\mathbf{x},0)$, the resulting smeared field has a Gaussian shape $q'^{(n)}(t,\mathbf{x}) \propto \exp(-|\mathbf{x}|^2/4\sigma^2)$, with

$$\sigma^2 \approx a^2 n \frac{\kappa}{1+6\kappa}. \tag{6}$$

The width σ in Eq. (6) defines the so-called smearing radius, which is a characteristic length of the procedure and it is proportional to n.

In this proceedings, we study how to tune σ for optimal performance, considering pseudoscalar and vector mesonic two-point functions, both at zero and non-zero three-momentum $\mathbf{p}$. The importance of choosing optimal smearing parameters is shown in Fig. 1, where the D meson effective energy reaches a plateau at smaller times in the case of the optimized smearing, performed through the method described in Sec. 2, compared to the other curves. We use gauge configurations produced by the European Twisted Mass Collaboration (ETMC) with $N_f = 2+1+1$ dynamical quarks on a set of gauge configurations, corresponding to a lattice spacing $a = 0.0907593$ fm and time and spatial extensions of the Lattice $T/a = 64$ and $L/a = 32$, respectively.

am_q	q \ q'	l	s	c	h_1	h_2
0.003	l	π, ρ	K, K^*	D, D^*	H_{1l}, H^*_{1l}	H_{2l}, H^*_{2l}
0.02	s		η_s, ϕ	D_s, D^*_s	H_{1s}, H^*_{1s}	H_{2s}, H^*_{2s}
0.275	c			η_c, J/ψ	H_{1c}, H^*_{1c}	H_{2c}, H^*_{2c}
0.357	h_1				H_{1h_1}, $H^*_{1h_1}$	H_{2h_1}, $H^*_{2h_1}$
0.550	h_2					H_{2h_2}, $H^*_{2h_2}$

Table 1: Pseudoscalar and vector mesons used in our analysis and their valence quarks. In the first column, we reported the bare masses of the quarks, as well.

2. Optimization strategy

We compute the effective energy for all the pseudoscalar and vector mesons in Tab. 1. The quarks h_1 and h_2 have bare masses $m_{h_1} = 1.3m_c$ and $m_{h_2} = 2m_c$, respectively. We use smeared interpolators corresponding to different values of n and fixed intensity $\kappa = 0.4$. In the following, to make explicit the parametric dependence of the effective energy on the smearing radius, we adopt the notation $E(t|\sigma)$.
We study both the cases $\mathbf{p} = 0$ and $\mathbf{p} \neq 0$. For $\mathbf{p} \neq 0$, the analysis is performed only for the mesons contained in the upper left 3×3 subset of Tab. 1, combining l, s and c quarks.
The momentum is injected using non-periodic boundary conditions for quark fields (see Ref. [6]), such that

$$q(t, \mathbf{x} + \mathbf{n}L) = \exp(i2\pi\mathbf{n} \cdot \boldsymbol{\theta_q}) q(t, \mathbf{x}), \qquad q(t + T, \mathbf{x}) = -q(t, \mathbf{x}). \tag{7}$$

In terms of the angles $\boldsymbol{\theta_q}$, the momentum carried by the mesons is given by

$$\mathbf{p} = \frac{2\pi}{L}(\boldsymbol{\theta_q} - \boldsymbol{\theta_{q'}}) = \frac{2\pi}{L}\boldsymbol{\theta}, \qquad \boldsymbol{\theta_{q^{(\prime)}}} = \theta_{q^{(\prime)}}(1,1,1), \qquad \boldsymbol{\theta} = \boldsymbol{\theta_q} - \boldsymbol{\theta_{q'}} = \theta(1,1,1), \tag{8}$$

where $\boldsymbol{\theta_q}$ ($\boldsymbol{\theta_{q'}}$) defines the boundary conditions of Eq. (7) for the $q(t, \mathbf{x})$ and $q'(t, \mathbf{x})$ quark fields, respectively. The usage of twisted boundary conditions automatically implements the so-called "momentum smearing" technique, recently proposed in Ref. [4], as it will be discussed in a future publication. The optimization of the smearing is carried out through the following steps:
we first, fix a certain time t^* where the effective energy has not reached a plateau yet.
Then, we determine the energy E_0 of the ground state from the large-time behaviour of the effective energy. Finally, we define the functional $\mathcal{F}(\sigma)$ as

$$\mathcal{F}(\sigma) = \frac{E(t^*|\sigma) - E_0}{E(t^*|\sigma = 0) - E_0}. \tag{9}$$

The functional $\mathcal{F}(\sigma)$ in Eq. (9) can be visualized as the ratio between the heights of the two rectangles N and D in Fig. 1 and it gives a measure of the relative magnitude of the contributions of the excited states at time t^*, with respect to the one present for $\sigma = 0$. The smaller the value of $\mathcal{F}(\sigma)$, the smaller the size of the unwanted excited state contaminations. The behaviour of the functional $\mathcal{F}(\sigma)$ as a function of σ is shown in Fig. 2, in the case of D, η_c and K mesons and for $t^*/a = 5$ and $\mathbf{p} = 0$. $\mathcal{F}(\sigma)$ lies between 0 and 1 for several values of the smearing radius,

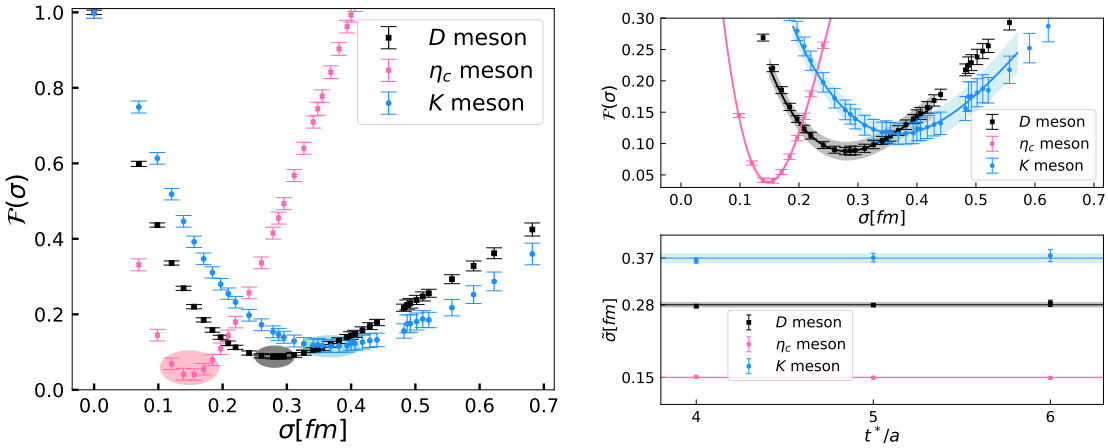

Figure 2: Left panel: optimizing functional for the D (black), η_c (pink) and K (blue) mesons at rest and $t^*/a = 5$. For each of the curves, we highlight the area around the minimum. Right panel: fit results around the minimum of the functional (top picture) and the dependence of the point of minimum $\tilde{\sigma}$ on t^* (bottom picture). Here, the sharp line is the optimal smearing radius $\overline{\sigma}$ for the corresponding meson, while the shaded bands its error inclusive of both statistical and systematic uncertainties.

which shows that the use of the Wuppertal smearing actually reduces the overlap with the excited states. The functional exhibits a minimum, which we refer to as $\tilde{\sigma}$, confirming that a tuning of the convolution steps is necessary to obtain the most benefit from the smearing. Moreover, $\tilde{\sigma}$ shifts as we change the meson. This behaviour will be discussed extensively in Sec. 3.
We fit the functional with a polynomial Ansatz to localize the point of minimum

$$\mathcal{F}(\sigma) = \mathcal{F}(\tilde{\sigma}) + \omega(\sigma - \tilde{\sigma})^2 + \nu(\sigma - \tilde{\sigma})^3, \qquad \sigma \in [\sigma_{\min}, \sigma_{\max}], \tag{10}$$

with $\sigma_{\min}$, $\sigma_{\max}$ defines an interval around the minimum of $\mathcal{F}(\sigma)$ depending on the specific meson, and $\mathcal{F}(\tilde{\sigma})$, ω, ν, $\tilde{\sigma}$ are fit parameters. The results of the fits are shown in the right panel of Fig. 2, where also the dependence of the minimum on the choice of t^* is reported. To take into account this small dependence, we define our estimator of the optimal smearing radius $\overline{\sigma}$ as the mean between the maximum and minimum values reached by $\tilde{\sigma}$ as a function of t^*, while the semi-difference of the two values is used as a systematic error. Then, after having found the optimal smearing radius, we use Eq. (6) to determine the number of convolution steps that minimize the overlap with the excited states.

3. Numerical results

The values assumed by the optimizing functional at its minimum are shown in the picture at the bottom of Fig. 3 for the pseudoscalar mesons and with $t^*/a = 4$. From its definition in Eq. (9), the functional $\mathcal{F}(\tilde{\sigma})$ can be used as an estimate of the suppression of the excited states due to the tuning of the smearing radius compared to the non-smeared case. Then, Fig. 3 tells us that the systems that benefit most from the smearing are the so-called heavy-light mesons, such as $D^{(*)}_{(s)}$, $H^{(*)}_{1l(s)}$ and $H^{(*)}_{2l(s)}$.

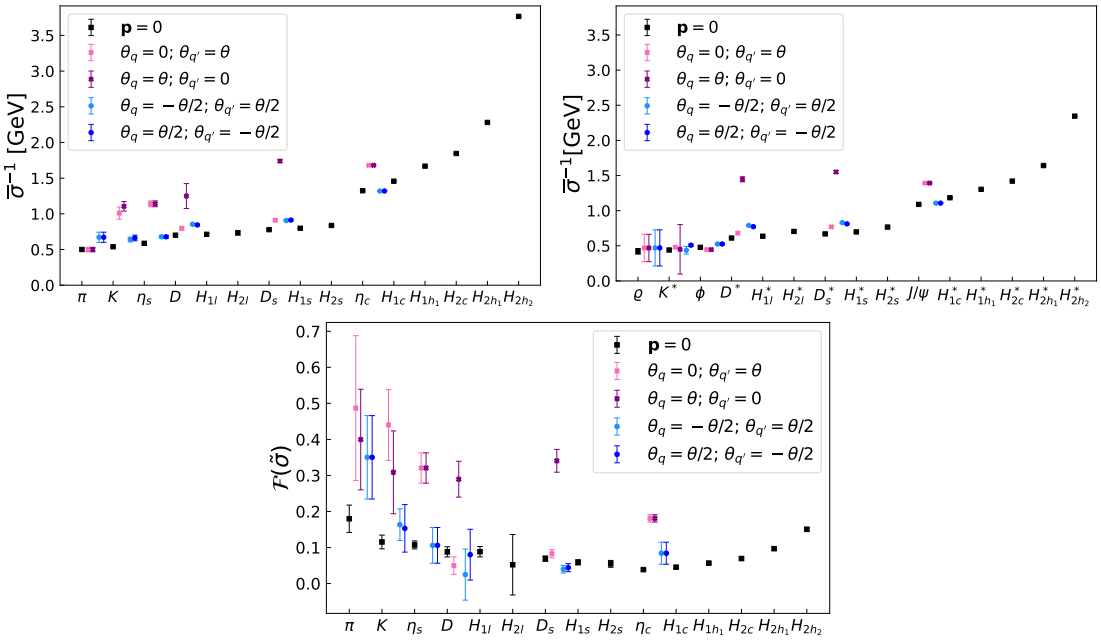

Figure 3: Top panels: inverse of the optimal smearing radius for the pseudoscalar and vector mesons, from left to right. Bottom panel: minima of the optimizing functional for the various pseudoscalar mesons and $t^*/a = 4$. The notation is the same of Tab. 1. Different colors correspond to different ways to assign the momentum of the meson among the valence quarks through twisted boundary conditions: mesons at rest (black points), all the momentum carried by the q' (pink points) and q quarks (purple points), momentum distributed equally among the quarks (light and dark blue points). Symbols are shifted to the right for clarity.

It is interesting to compare different ways to assign the momentum between the quarks through the twisted boundary conditions in Eq. (7), when its magnitude is fixed $\theta = 1.97$. The optimal configuration for mesons with identical valence quarks (i.e. π, η_s, η_c) is realized when the latter carry the same fraction of momentum $\theta/2$. On the other hand, the values of the functional at its minimum for the D and D_s mesons become $3-4$ times smaller when passing from a setup where the light quark carries all the momentum $\theta_q = \theta$ (purple points), to one where we give to the charm quark all the momentum $\theta_{q'} = \theta$ (pink points). This can be interpreted in a natural way by assuming that the fraction of $\mathbf{p}$ carried by the valence quarks increases with their masses. Thus, if the quarks are degenerate we expect the momentum distribution to be symmetric, while for heavy-light mesons, such as $D_{(s)}$, the heavier charm quark is expected to bear the largest part of $\mathbf{p}$. The pictures at the top of Fig. 3 present the inverse of the optimal smearing radius $\overline{\sigma}^{-1}$ for the pseudoscalar and vector mesons. For $D_{(s)}$ mesons, the case where $\mathbf{p}$ is assigned entirely to the light quark (purple points) is the only setup where $\overline{\sigma}^{-1}$ increases significantly, while it is approximately the same for the other three kinds of momentum distribution. Applying this observation to the mesons at rest, we propose to parametrize $\overline{\sigma}^{-1}$ as a function of the reduced masses of the valence quarks of the mesons. In this way, we have as an independent variable a quantity that is mostly sensitive to the light quark for the heavy-light mesons.

We use a quark constituent model to obtain the masses of the valence quarks. Under this assumption, the color string forces produce a spin-independent potential that confines the quarks. Then, the

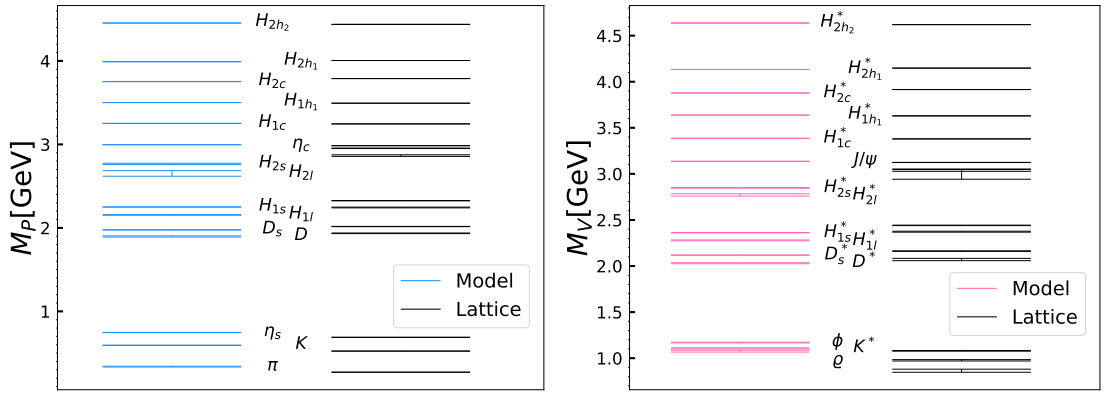

Figure 4: Spectrum of the pseudoscalar (left picture) and vector (right picture) mesons at rest, obtained from the quark constituent model (blue and pink lines) and from the lattice (black lines) through the fitted values of the plateaux of the effective masses.

m_q [MeV]	$\kappa_{qq'}$ [MeV]	l	s	c	h	h_2
445(4)	l	369(6)	256(4)	66(5)	61(3)	59(22)
531(1)	s		212(2)	71(1)	56(1)	41(6)
1548.4(2)	c			69.9(3)	66.9(2)	62.5(3)
1798.9(2)	h				68.0(2)	71.1(2)
2292.0(2)	h_2					91.1(2)

Table 2: Quark constituent masses and $\kappa_{qq'}$ energies fitted from the values of the effective masses of the mesons at their plateaux.

residual interactions between the quarks q and q' can be described by a color-magnetic, spin-spin Hamiltonian [7, 8], which for mesons at rest reads

$$H_{qq'} = m_q + m_{q'} + 2\kappa_{qq'}\mathbf{S_q}\cdot\mathbf{S_{q'}}, \tag{11}$$

where $m_{q,q'}$ are the so-called quark constituent masses of the q and q' quarks, respectively, and the energies $\kappa_{qq'}$ depend on the flavour structures of the mesons, as well as on the color state of the quark pairs, while $\mathbf{S}_{q,q'}$ are the spins of the quarks. Eq. (11) provides a very simple mass formula for mesons at rest and with zero orbital angular momentum, given by

$$M_{\mathrm{P(V)}} = m_q + m_{q'} + \kappa_{qq'}\left[J_{\mathrm{P(V)}}(J_{\mathrm{P(V)}}+1) - \frac{3}{2}\right], \tag{12}$$

with J being the total angular momentum, such that $J_{\mathrm{P}} = 0$ and $J_{\mathrm{V}} = 1$ for pseudoscalar (P) and vector (V) mesons, respectively. Then, we can combine the masses of the pseudoscalar and vector mesons in Eq. (12) to get simple expressions for the parameters of the model

$$\begin{aligned} M_{\mathrm{V}} + \frac{1}{3}M_{\mathrm{P}} &= \frac{4}{3}(m_q + m_{q'}), \\ M_{\mathrm{V}} - M_{\mathrm{P}} &= 2\kappa_{qq'}. \end{aligned} \tag{13}$$

The quark constituent masses and the $\kappa_{qq'}$ coefficients are fitted using the relations in Eq. (13) and employing for $M_{\mathrm{P(V)}}$ the values obtained from the effective energies of the mesons at rest, also

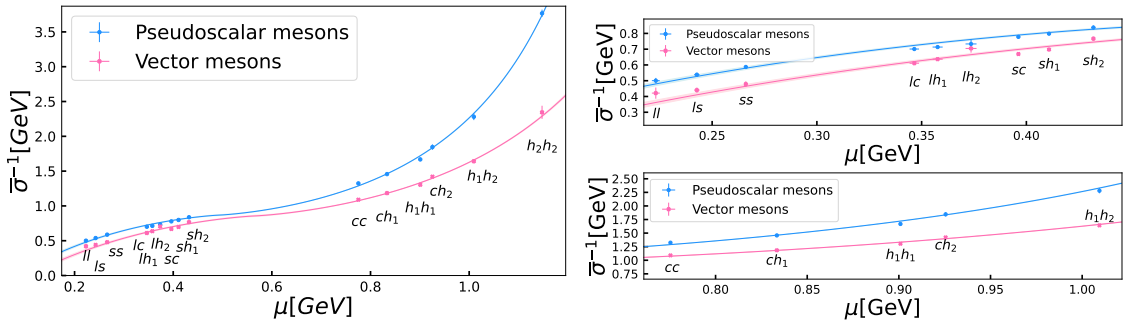

Figure 5: Left panel: inverse of the optimal smearing radius as function of the reduced constituent masses of the valence quarks of the mesons and fit results for pseudoscalar (blue line and points) and vector (pink line and points) mesons at rest. Right panel: zoom in on the fit regions. In both the pictures we report the quark contents of the mesons to make them easier to read. The notation is the same of Tab. 1.

	A	μ^* [GeV]	Λ [GeV]	B [GeV]
P	0.264(4)	0.493(5)	1.007(7)	0.868(8)
V	0.270(6)	0.565(6)	1.24(3)	0.86(1)

Table 3: Parameters describing the dependence of the inverse of the optimal smearing radius as a function of the reduced masses of the valence quarks of the mesons, obtained from a quark constituent model. The parameters are obtained by fitting separately the data for the pseudoscalar (P) and vector (V) mesons.

known as effective masses.

Fig. 4 shows that the model reproduces well the observed mass hierarchy of the mesons, besides the $H^{(*)}_{2l(s)}$ and ρ mesons.

Fig. 5 shows that the optimal smearing radius exhibits a monotonic increasing behaviour as a function of the reduced masses of the mesons μ, obtained from the values in Tab. 2.

At low energies, $\mu < 0.6$ GeV, $\overline{\sigma}^{-1}$ shows a linear behaviour for both pseudoscalar and vector mesons $\overline{\sigma}^{-1} \propto \mu$. For $\mu > 0.6$ GeV, the optimal smearing radius scales as a logarithmic function $\overline{\sigma}^{-1} \propto -1/\ln(\mu^2)$. Thus, we choose to parametrize the optimal smearing radius with a heuristic Ansatz of the form

$$f(\mu) = (\mu^* - \mu)\frac{1}{A\ln(\frac{\mu-\mu^*}{\Lambda})^2} + B, \tag{14}$$

to recover both the low and high-energy regimes.

Then, we fit the inverse of the optimal smearing radius for the pseudoscalar and vector mesons, separately, through Eq. (14) to determine the free parameters: three energy scales μ^*, B, Λ, and one dimentionless coefficient A. The results are reported in Tab. 3, while the corresponding curves are depicted in Fig. 5. The latter follows very closely the points as shown by the zooms in on the fit regions and we get values of the reduced chi-squared given by $\chi^2_{\rm P} = 0.75$ and $\chi^2_{\rm V} = 0.46$ for pseudoscalar and vector mesons, respectively.

4. Conclusions

This work presented an optimization of the Wuppertal smearing to isolate ground states of pseudoscalar and vector mesons at rest and in motion, realized by tuning the smearing radius to minimize an optimizing functional.
The latter is defined as the difference between the effective energy computed at a time where the excited states are supposed to be dominant, and its value at the plateau. By definition, smaller values of this functional correspond to two-point functions where the contribution of the ground state can be isolated at smaller times.
The optimizing functional exhibits a minimum at non-zero values of the smearing radius, as shown in Fig. 2. Thus, the smearing always helps to suppress the contributions of the excited states and the greatest suppression is achieved for heavy-light mesons, as shown by the picture at the bottom of Fig. 3.
We investigated the efficiency of the smearing when changing the distribution of the momentum of the meson among the quarks. The results are shown in the figures at the top of Fig. 3. For mesons with identical valence quarks, the optimal solution is to split the momentum of the meson equally between the quarks. For heavy-light mesons, the smearing is more efficient if the heavy quark carries a larger fraction of the momentum.
We defined the optimal smearing radius $\overline{\sigma}$ through the point of minimum of the optimizing functional. The inverse of the optimal smearing radius, for mesons at rest, presented a monotonic increasing behaviour as a function of the reduced constituent masses of the valence quarks of the mesons, described very well by a product of a linear function and a logarithmic scaling, as can be seen from Fig. 5.
This behaviour allows us to determine the optimal smearing radius across a broad range of reduced masses, corresponding to different kinds of mesons. Thus, optimizing the smearing will be very helpful to us in tackling problems where it is crucial to anticipate the signal as much as possible, such as the semileptonic decays of the B mesons, which would obtain also the most benefit from it being themselves heavy-light mesons.

References

[1] G. Parisi, *The strategy for computing the hadronic mass spectrum*, *Physics Reports* **103** (1984) 203.

[2] G.P. Lepage, *The Analysis of Algorithms for Lattice Field Theory*, in *Theoretical Advanced Study Institute in Elementary Particle Physics*, 6, 1989.

[3] S. Güsken, *A study of smearing techniques for hadron correlation functions*, *Nuclear Physics B - Proceedings Supplements* **17** (1990) 361.

[4] G.S. Bali, B. Lang, B.U. Musch and A. Schäfer, *Novel quark smearing for hadrons with high momenta in lattice QCD*, *Phys. Rev. D* **93** (2016) 094515 [1602.05525].

[5] M. Albanese, F. Costantini, G. Fiorentini, F. Flore, M. Lombardo, R. Tripiccione et al., *Glueball masses and string tension in lattice qcd*, *Physics Letters B* **192** (1987) 163.

[6] G. de Divitiis, R. Petronzio and N. Tantalo, *On the discretization of physical momenta in lattice qcd*, *Physics Letters B* **595** (2004) 408.

[7] M. Frank and P.J. O'Donnell, *Constituent Quarks, Soft Pions and Meson Masses*, *Z. Phys. C* **34** (1987) 39.

[8] L. Maiani, F. Piccinini, A.D. Polosa and V. Riquer, *Diquark-antidiquark states with hidden or open charm and the nature of $x(3872)$*, *Phys. Rev. D* **71** (2005) 014028.